Model-plant mismatch detection and model update for a run-of-mine ore milling circuit under model predictive control✩

L.E. Olivier[a], I.K. Craig[a,*]

[a]*Department of Electrical, Electronic, and Computer Engineering, University of Pretoria, Pretoria, South Africa.*

Abstract

The performance of a model predictive controller depends on the quality of the plant model that is available. Often parameters in a run-of-mine (ROM) ore milling circuit are uncertain and inaccurate parameter estimation leads to a mismatch between the model and the actual plant. Although model-plant mismatch is inevitable, timely detection of significant mismatch is desirable. Once significant mismatch is detected the model may be partially re-identified in order to prevent deteriorated control performance. This paper presents a simulation study of the detection of mismatch in the parameters of a ROM ore milling circuit model using a partial correlation analysis approach. The location of the mismatch in the MIMO model matrix is correctly detected, and the process model subsequently updated.

Keywords:

Milling circuit, model-plant mismatch, model predictive control, model update, partial re-identification, run-of-mine (ROM) ore

---

1. Introduction

Grinding mill circuits are still predominantly controlled using single-loop PI(D) controllers [1] despite the significant advances that a technology such as model predictive control (MPC) has made in the process industries [2]. Perhaps one of the reasons for this is the fact that the dynamics of milling circuits can change significantly over time leading to deteriorating controller performance.

Milling circuits, and mineral processing operations in general, are often affected by poor modelling [3]. For such processes, it is stated by [3] that the peripheral control tools (which includes observers, data reconciliation, soft sensors and model parameter tuners) are as important as the controller itself. MPC controllers are also known to not produce very good results in the presence of significant model-plant mismatch [4, 5]. A technology that may aid the introduction of advanced control in grinding mill circuits is model-plant mismatch detection ([6, 7]), as described in this paper.

The aim of the mismatch detection strategy is to locate the specific transfer function element(s) in the model transfer function matrix that contain significant mismatch. Once significant mismatch has been detected, re-identification of the particular part of the plant model that contains the mismatch may be done. This partial re-identification would be much less costly and time-consuming than full process re-identification ([8]). The controller can then be redesigned based on the updated model. These steps could

2

be performed either by the control engineer, or via an automatic model update strategy. Care should however be taken when making use of the latter method.

This paper describes a simulation study of the application of a model-plant mismatch detection strategy described in [6], to a ROM ore milling circuit under MPC control. The milling circuit model used is a linear time-invariant (LTI) approximation of a fundamental milling circuit model described in [9]. Model-plant mismatch, motivated from industrial experiments [10], is introduced in the model and its location in the multivariable matrix model is correctly detected. The model is then automatically updated and the controller redesigned. The results will show how the automatic model update strategy can help to improve controller performance.

2. ROM ore milling circuit

This section gives a brief introduction to the ROM ore milling operation considered in this work. The discussion is based on a single stage semi-autogenous mill operated in closed circuit with a hydrocyclone.

Ore bearing some valuable mineral is fed to the milling circuit at about 100 tons/hour. The ore is ground down to product with a particle size of 80% smaller than 75 μm ($P_{80} = 75\mu$m). A hydrocyclone is used in closed circuit with the mill to separate the product from the out-of-specification material. The valuable mineral is then extracted downstream through a leaching or floatation process.

The feed to the mill (see Fig. 1) constitute the underflow of the cyclone, feed ore, water and steel balls. Steel balls are usually added in discrete

3

quantities by the operator but in this study it will be treated as a continuous variable. The mill discharges the ground slurry into a sump through an end-discharge grate. The slurry is diluted with water in the sump and pumped to the hydrocyclone for classification. The product of the milling circuit is the overflow of the hydrocyclone.

The controlled variables in the milling circuit are the product particle size (PSE), the fraction of the mill volume filled with material (LOAD), and the volume of slurry in the sump (SLEV). The manipulated variables are the feed-rate of solids into the mill (MFS), the feed-rate of water into the mill (MIW), the feed-rate of steel balls into the mill (MFB), the flow-rate of water into the sump (SFW), and the flow-rate of slurry into the hydrocyclone (CFF). The operating point of the milling circuit and constraints on the variables are given in the nomenclature table.

2.1. Non-linear mill model

The milling circuit model is based on phenomenological equations and consists of separate modules for the feeder, mill, sump and hydrocyclone such that arbitrary circuit topologies may be constructed. The model uses five states, namely water, rocks, solids, fines, and steel balls to describe the flow of material through the milling circuit. All the equations that constitute the non-linear model are based on these material classifications. A full description of these equations can be found in [9]. Here details are only provided for the mill module that contains the parameters which usually give rise to model-plant mismatch. These changes in the plant are later detected by the model-plant mismatch detection algorithm.

The mill module is capable of modelling various mill types e.g. ball, SAG
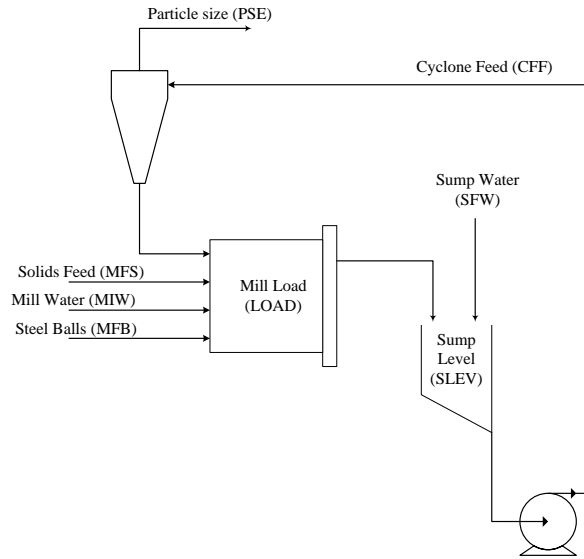
4

Figure 1: ROM ore milling circuit

(semi-autogenous grinding) and AG (autogenous grinding) mills. The model adds the effects of mill power and slurry rheology (as described by [11]) to the breakage and power functions.

The mill has five states, which are the holdups of the five classifications of material in the mill, namely water, rocks, solids, fines, and steel balls. The

Nomenclature						
	Minimum	Maximum	Nominal	%Δ	W	Description
Variables						
MIW	0	100	33.33		-	Flow-rate of water to the mill $[\frac{\mathrm{m}^3}{\mathrm{h}}]$
MFS	0	200	100		0.1	Flow-rate of solids to the mill $[\frac{\mathrm{t}}{\mathrm{h}}]$
MFB	0	4	2		-	Flow-rate of steel balls to the mill $[\frac{\mathrm{t}}{\mathrm{h}}]$
CFF	400	500	442		0.1	Flow-rate of slurry to the cyclone $[\frac{\mathrm{m}^3}{\mathrm{h}}]$
SFW	0	400	267		0.1	Flow-rate of water to the sump $[\frac{\mathrm{m}^3}{\mathrm{h}}]$
PSE	60	90	80		100	Product particle size [% < 75μm]
LOAD	30	50	45		100	Total charge of the mill [%]
SLEV	2	37.5	30		1	Level of the sump [m^3]
Internal flows						
V_{wi}, V_{wo}						Flow of water into/out of the mill $[\frac{\mathrm{m}^3}{\mathrm{h}}]$
V_{si}, V_{so}						Flow of solids into/out of the mill $[\frac{\mathrm{m}^3}{\mathrm{h}}]$
V_{fi}, V_{fo}						Flow of fines into/out of the mill $[\frac{\mathrm{m}^3}{\mathrm{h}}]$
V_{ri}, V_{ro}						Flow of rocks into the mill $[\frac{\mathrm{m}^3}{\mathrm{h}}]$
V_{bi}, V_{bo}						Flow of steel balls into the mill $[\frac{\mathrm{m}^3}{\mathrm{h}}]$
States						
X_{mw}	0	50	8.53			Holdup of water in the mill [m^3]
X_{ms}	0	50	9.47			Holdup of solid ore in the mill [m^3]
X_{mf}	0	50	3.54			Holdup of fine ore in the mill [m^3]
X_{mr}	0	50	20.25			Holdup of rocks in the mill [m^3]
X_{mb}	0	20	6.75			Holdup of steel balls in the mill [m^3]
Parameters						
α_f	0.05	0.15	0.1	50		Fraction of fines in the ore [dimensionless]
α_r	0.05	0.15	0.1	50		Fraction of rocks in the ore [dimensionless]
ϕ_f	14	42	28	50		Power needed per ton of fines produced $[\frac{\mathrm{kW \cdot h}}{\mathrm{t}}]$
ϕ_r	55	83	69	20		Rock abrasion factor $[\frac{\mathrm{kW \cdot h}}{\mathrm{t}}]$
ϕ_b	89	99	94	5		Steel abrasion factor $[\frac{\mathrm{kW \cdot h}}{\mathrm{t}}]$
Constants						
ε_{ws}			0.6			Maximum water-to-solids volumetric flow at zero pulp flow [dimensionless]
V_V			40			Volumetric flow per "flowing volume" driving force [h^{-1}]
$P_{\max}$			2000			Maximum mill motor power [kW]
δ_{P_v}			1			Power change parameter for volume [dimensionless]
δ_{P_s}			1			Power change parameter for fraction solids [dimensionless]
$v_{\mathrm{P_{max}}}$			0.45			Fraction of mill volume filled for maximum power [dimensionless]
$\varphi_{\mathrm{P_{max}}}$			0.51			Rheology factor for maximum mill power [dimensionless]
α_P			0.82			Fractional power reduction per fractional reduction from maximum mill speed [dimensionless]
v_{mill}			100			Mill volume [m^3]
α_{ϕ_f}			0.01			Fractional change in kW/fines produced per change in fractional filling of mill [dimensionless]
χ_P			0			Cross term for maximum power [dimensionless]

state equations are given by

$$\dot{X}_{mw} = MIW - V_{wo} \tag{1}$$

$$\dot{X}_{ms} = \frac{MFS}{D_s}(1 - \alpha_r) - V_{so} + RC \tag{2}$$

$$\dot{X}_{mf} = \alpha_f \frac{MFS}{D_s} - V_{fo} + FP \tag{3}$$

$$\dot{X}_{mr} = \alpha_r \frac{MFS}{D_s} - RC \tag{4}$$

$$\dot{X}_{mb} = \frac{MFB}{D_b} - BC \tag{5}$$

where each of the feed streams has been replaced by its respective expression; RC is the amount of rocks consumed,

$$RC \triangleq \frac{1}{D_s \phi_r} \cdot P_{\text{mill}} \cdot \varphi \cdot \left(\frac{X_{mr}}{X_{mr} + X_{ms}} \right), \tag{6}$$

BC is the amount of balls consumed,

$$BC \triangleq \frac{1}{D_b \phi_b} \cdot P_{\text{mill}} \cdot \varphi \cdot \left(\frac{X_{mr}}{X_{mr} + X_{ms}} \right), \tag{7}$$

FP is the amount of fines produced,

$$FP \triangleq \frac{P_{\text{mill}}}{D_s \phi_f \left[1 + \alpha_{\phi_f} \left(\frac{LOAD}{v_{\text{mill}}} - v_{\text{P}_{\max}} \right) \right]}, \tag{8}$$

and the flows out of the mill are given by

$$V_{wo} = V_V \cdot \varphi \cdot X_{mw} \left(\frac{X_{mw}}{X_{mw} + X_{ms}} \right) \tag{9}$$

$$V_{so} = V_V \cdot \varphi \cdot X_{mw} \left(\frac{X_{ms}}{X_{mw} + X_{ms}} \right) \tag{10}$$

$$V_{fo} = V_V \cdot \varphi \cdot X_{mw} \left(\frac{X_{mf}}{X_{mr} + X_{ms}} \right) \tag{11}$$

where φ is the rheology factor

$$\varphi \triangleq \sqrt{\frac{\max\left[0, \left(X_{mw} - \left(\frac{1}{\varepsilon_{ws}} - 1\right) X_{ms}\right)\right]}{X_{mw}}}. \tag{12}$$

No rocks or steel balls can exit the mill as they are restricted by the discharge grate. Two other important expressions contained in the milling equations are the total charge in the mill ($LOAD$) and the power drawn from the mill motor (P_{mill}) given by

$$
\begin{aligned}
LOAD &= X_{mw} + X_{ms} + X_{mr} + X_{mb} \tag{13} \\
P_{\text{mill}} &= P_{\max} \cdot \{1 - \delta_{P_v} Z_x^2 \\
&\quad -2\chi_p \delta_{P_v} \delta_{P_s} Z_x Z_r - \delta_{P_s} Z_r^2\}, \tag{14}
\end{aligned}
$$

where Z_x is the effect of the load on the power consumption defined as $Z_x \triangleq (X_{mw} + X_{ms} + X_{mr} + X_{mb})/(v_{\text{P}_{\max}} \cdot v_{\text{mill}} - 1)$ and Z_r is the effect of the rheology on power consumption defined as $Z_r \triangleq (\varphi/\varphi_{\text{P}_{\max}}) - 1$. All the other parameters and constants in the milling equations are listed in the nomenclature table.

2.2. Linearized milling circuit model

The milling circuit is controlled by a linear model predictive controller, which is described in the next section. The controller requires a linear model of the plant that is obtained through applying a standard system identification (SID) procedure as described by [12], to the milling circuit model described by [9]. Step tests were performed around the operating point of the milling circuit. Operating data for 60 hours were collected and models

were fitted for all 9 elements of the transfer function matrix. The final model for control is then given by:

$$
\begin{bmatrix} \Delta PSE \\ \Delta LOAD \\ \Delta SLEV \end{bmatrix} = \begin{bmatrix} g_{11} & g_{12} & g_{13} \\ g_{21} & g_{22} & g_{23} \\ g_{31} & g_{32} & g_{33} \end{bmatrix} \begin{bmatrix} \Delta CFF \\ \Delta MFS \\ \Delta SFW \end{bmatrix} \tag{15}
$$

where g_{1j} is in the form

$$
g_{1j} = \frac{k_{1j}}{s + \alpha_{1j}} e^{-\theta_{1j}s} \tag{16}
$$

with $k_{11} = -2.4 \times 10^{-4}$, $k_{12} = -5.99 \times 10^{-4}$, $k_{13} = 1.45 \times 10^{-3}$; $\alpha_{11} = 0.5882$, $\alpha_{12} = 1.353$, $\alpha_{13} = 2.216$; and $\theta_{11} = 0.0111$, $\theta_{12} = 0.0639$, $\theta_{13} = 0.0111$.

The other 6 transfer functions are in the form

$$
g_{ij} = \frac{k_{ij}}{s + 10^{-6}} \tag{17}
$$

with $k_{21} = 7.15 \times 10^{-4}$, $k_{22} = 7.22 \times 10^{-3}$, $k_{23} = -1.39 \times 10^{-3}$, $k_{31} = -0.60$, $k_{32} = 0.0097$, and $k_{33} = 0.774$. Here we have used the form $g_{ij} = \frac{k_{ij}}{s + \varepsilon}$ where $\varepsilon \to 0$ to approximate an integrator with a first order model. The models were derived in time units of hours with a sampling time of 10 seconds.

The model does not contain reference to the manipulated variables MIW and MFB. In this study the value of MFB is kept constant at its nominal value (as reported in the nomenclature table). The value of MIW is derived from the value of MFS through a constant water to solids ratio into the mill as discussed by [13].

3. Controller design

The controller for the milling circuit is a linear model predictive controller based on the linearized plant model discussed in the previous section. At each

9

sampling instant the objective of the controller is to minimize some scalar performance index

$$\min_{u} V(u, x_0) \tag{18}$$

$$s.t. \ x \in X, u \in U \tag{19}$$

$$\theta_c(x, u) \leq 0 \tag{20}$$

where $x : \mathbb{R} \to \mathbb{R}^{n_x}$ is the state trajectory, $u : \mathbb{R} \to \mathbb{R}^{n_u}$ is the control trajectory, x_0 is the initial state and $\theta_c(x, u)$ is the constraint vector. The solution to the optimization problem provides a set of optimal control moves, the first of which is implemented and the optimization problem is again solved at the next sampling instant.

At each sampling instant the controller calculates the required values for the manipulated variables CFF, SFW and MFS. The prediction horizon should be chosen large enough to capture the dynamics of the model, but small enough such that the control action calculation is not too computationally expensive. The control horizon should be chosen small enough such that the controller is not too aggressive, but large enough such that a sufficient part of the prediction horizon contains control action. The controller uses a prediction horizon of 800 (covering 2.22 hours which is close to the longest time constant in (16)) and a control horizon of 100 to cover a sufficient part of the prediction horizon. In order however to ensure that the controller is not too aggressive blocking is used by only allowing the controller to change its output every fifth step. With these parameters sufficient performance is attained (see Fig. 2) and the aforementioned conditions are satisfied. The constraints imposed by the controller, as well as the weights given to each controlled and manipulated variable are as shown in the nomenclature table.
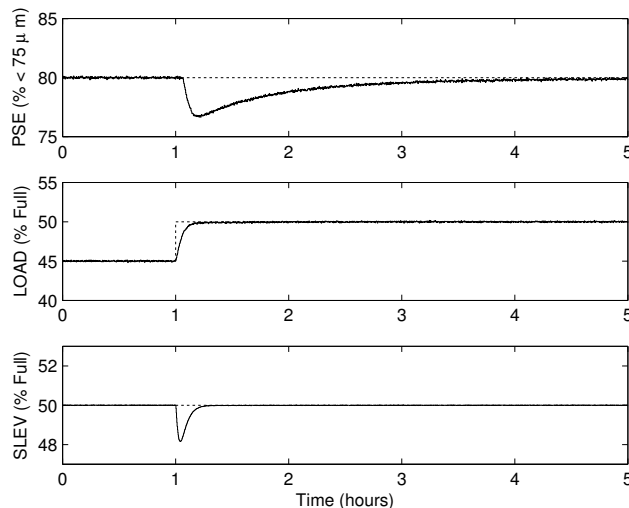
10

Figure 2: Nominal operation data

The Model Predictive Control toolbox in MATLAB ([14]) is then used to define the controller.

The simulation results in Fig. 2 show the nominal operation (without any parameter mismatch in the plant) of the controller over 5 hours. A set-point change is made for the LOAD from 45% to 50% at time 1 hour. This set-point change is rather large and would typically not be made during the normal operation of the milling circuit. This is similar to the set-point change later employed to ensure sufficient excitation for the model-plant mismatch detection algorithm. The set-points are indicated with dashed lines in the figure.

The values of the manipulated variables for nominal operation are shown in Fig. 3.

11
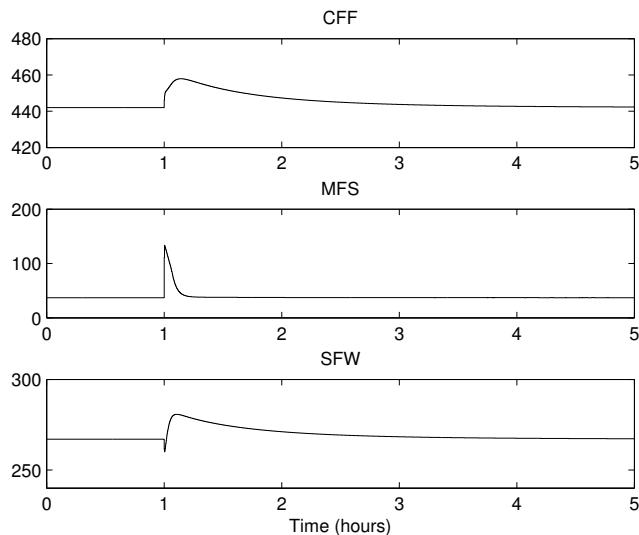
Figure 3: Manipulated variables for nominal operation

4. Model-plant mismatch detection

A model-plant mismatch identification technique is applied to the ROM ore milling circuit to detect differences between the available model and the actual plant. Recently [6] proposed a method for model-plant mismatch (MPM) detection in MPC applications based on a partial correlation analysis between the model residuals and the manipulated variables. Partial correlation analysis helps in detecting hidden correlations as well as inhibiting the detection of spurious correlations.

Consider the closed-loop internal model control (IMC) structure represented in Fig. 4 (from [15]). Here $\boldsymbol{G}$ is a $n \times m$ MIMO plant, $\hat{\boldsymbol{G}}$ is the model representing $\boldsymbol{G}$ and $\boldsymbol{Q}$ is a multivariable controller. The plant and model outputs are $\boldsymbol{y}(k)$ and $\hat{\boldsymbol{y}}(k)$ respectively, $\boldsymbol{r}(k)$ is the vector of references, $\boldsymbol{u}(k)$ the manipulated variables and $\boldsymbol{v}(k)$ the vector of disturbances.

12
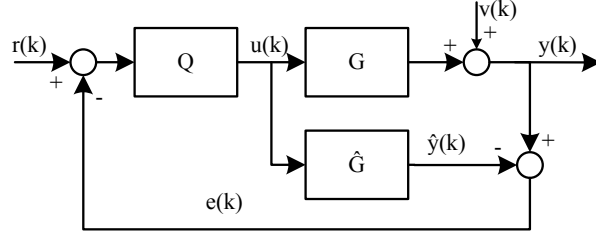
Figure 4: Closed-loop IMC structure

The residuals $(e(k))$ are given by

$$e(k) = y(k) - \hat{y}(k) = \Delta u(k) + v(k) \tag{21}$$

where $(\Delta = G - \hat{G})$ is the mismatch between the plant and the model. Correlation analysis between the signals $e(k)$ and $u(k)$ indicates the amount of mismatch Δ. The following relations are obtained from Fig. 4:

$$e(k) = [I + \Delta Q]^{-1} \Delta Q r(k) + [I + \Delta Q]^{-1} v(k) \tag{22}$$

$$u(k) = \underbrace{Q[I + \Delta Q]^{-1}}_{S_{ru}} r(k) - \underbrace{Q[I + \Delta Q]^{-1}}_{S_{vu}} v(k) \tag{23}$$

where S_{ru} and S_{vu} are the input sensitivities from r and v respectively.

At each sampling instant the values of the manipulated variables are calculated based on the difference between the output and the reference vectors. Depending on the interactions in the model and the design of the controller, correlation may exist between manipulated variables. This may lead to the detection of spurious correlation or to the non-detection of hidden correlation between residuals and manipulated variables. This would in turn obscure the correct identification of the location of significant MPM. To overcome this [6] proposed the use of partial correlation analysis.

13

Data for analysis should be chosen from a period of time where there is sufficient set-point excitation. Since models are fitted to the sensitivity functions $\boldsymbol{S}_{ru}$ and $\boldsymbol{S}_{vu}$, the set-points should be sufficiently exciting to ensure estimation accuracy. In order to ensure that MPM is not incorrectly identified due to the presence of disturbances, the disturbance free components of the manipulated variables are required. These are the components of the MVs needed to react to set-point changes and not for disturbance rejection. The disturbance free components of the MVs are represented as $\hat{\boldsymbol{u}}^r(k)$ and may be obtained as described by [6].

Next the component of each MV that is uncorrelated with all other MVs is computed. Each MV may be represented as

$$\hat{u}_i^r(k) = \boldsymbol{G}_{u_i}\tilde{\boldsymbol{u}}^r(k) + \epsilon_{u_i}(k) \tag{24}$$

where $\boldsymbol{G}_{ui}$ is a model identified between $\boldsymbol{u}_i^r$ and all the other MVs, $\tilde{\boldsymbol{u}}^r$ contains all the other MVs except for u_i and ϵ_{u_i} is that component of u_i that is uncorrelated with all other MVs. The estimate of ϵ_{u_i} is then given by:

$$\hat{\epsilon}_{u_i}(k) = \hat{u}_i^r(k) - \boldsymbol{G}_{u_i}\tilde{\boldsymbol{u}}^r(k) \tag{25}$$

A similar procedure is applied to calculate the component of each residual that is uncorrelated with all other MVs except u_i.

$$e_j(k) = \boldsymbol{G}_{e_j}\tilde{\boldsymbol{u}}^r(k) + \epsilon_{e_j}(k) \tag{26}$$

Here G_{e_j} is the model identified between residual e_j and all other MVs except u_i. The estimate for ϵ_{e_j} is then given by

$$\hat{\epsilon}_{e_j}(k) = e_j(k) - \boldsymbol{G}_{e_j}\tilde{\boldsymbol{u}}^r(k) \tag{27}$$

Non-zero correlation between $\hat{\epsilon}_{e_j}$ and $\hat{\epsilon}_{u_i}$ indicates the presence of model-plant mismatch in the $u_i - y_j$ channel. This model-plant mismatch identification technique is applied to the ROM ore milling circuit to detect mismatch between parameters in the model and the actual plant.

5. Model-plant mismatch detection for the milling circuit

When the parameter ϕ_f (see equation (8)), which is an estimate of the hardness of the ore being fed into the mill, is changed from its nominal value to some perturbed value in the plant ($\boldsymbol{G}$) while the nominal value is maintained in the model ($\hat{\boldsymbol{G}}$), there is a discrepancy between the actual hardness of the ore in the mill and the estimate of the hardness. The hardness of the ore entering the mill is a variable that commonly varies during operation of the milling circuit.

A discussed in section 2, the hardness of the ore entering the mill affects the hold-up time of ore in the mill. In the linear model, the hold-up time is approximately equal to the time constants in the transfer functions of LOAD/CFF (g_{21}) and LOAD/SFW (g_{23}). It has been shown ([10]) that the time constant is given by $\tau = RC$ where C is the volume of material inside the mill and R is the inverse of the slurry discharge rate. The relative uncertainties of the time constants in the linearized transfer function has been investigated by [10]. The relative uncertainty matrix for the time constants in the linearized model was found to be:

$$\tau_{ij} : \begin{bmatrix} 18\% & - & 19\% \\ 40\% & - & 60\% \\ - & - & - \end{bmatrix}.$$ (28)

15

With reference to this result the time constants for the transfer functions of LOAD/CFF and LOAD/SFW in the plant model are increased by 30%. The model-plant mismatch detection algorithm is now expected to detect this parameter mismatch in the perturbed transfer functions.

A simulation run is initially performed with the nominal plant over 5 hours. The model-plant mismatch algorithm correctly identifies no mismatch as no partial correlation between the residuals and the manipulated variables. This result is shown in Fig. 5. The model ($\hat{G}$) is then kept constant while the actual plant in the simulation (G) is perturbed. The time constants are increased in the transfer function elements g_{21} as well as g_{23} and a simulation run is performed (once again over a period of 5 hours). The model-plant mismatch detection algorithm is applied and the partial correlation plots are shown in Fig. 6. The 99 % confidence intervals for the correlations are shown in blue. For an industrial application the confidence intervals are not necessarily the best method of judging that significant mismatch is present. This is because it is often difficult to model the interactions perfectly in order to identify the correlation free components of each signal. A more appropriate way is to define a threshold value (e.g. ± 0.4) and only if the correlation exceeds this value is the mismatch judged to be significant.

From Fig. 6 it is seen that the mismatch in both (g_{21}) and (g_{23}) are correctly detected with clear non-zero correlation. More details about the models determined in calculating the component of each MV that is uncorrelated with all other MVs can be seen in Appendix A [7].

In order to ensure sufficient excitation in the generation of these results, which is one of the requirements for applying the MPM detection algorithm
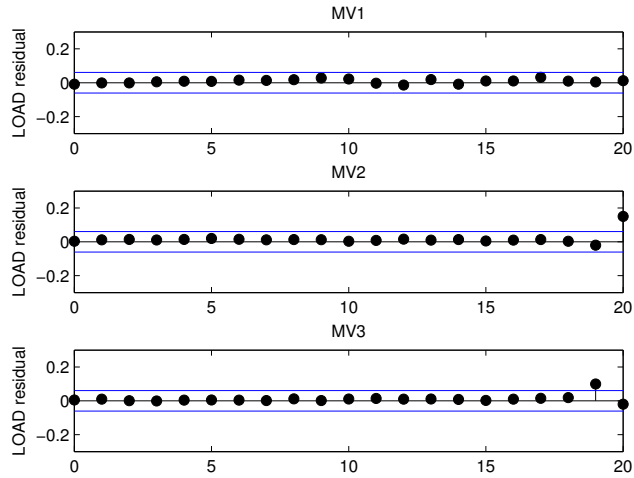
16

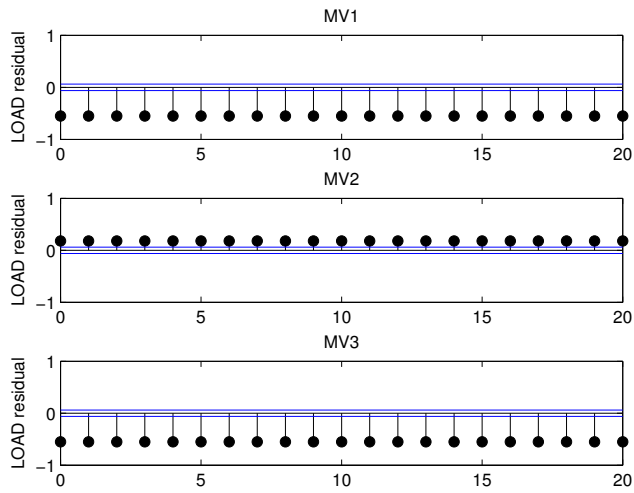Figure 5: Partial correlation plots between the MVs and the LOAD residual with no mismatch

Figure 6: Partial correlation plots between the MVs and the LOAD residual for time constant mismatch in g_{21} and g_{23}

17

of [6], the reference value for LOAD was changed from 45% to 50% at time 1 hour. The models $\boldsymbol{G}_{u_i}$ and $\boldsymbol{G}_{e_j}$ determined by the model-plant mismatch detection algorithm were based on the output error (OE) structure. The OE models were both specified with orders equal to 3.

Craig and MacLeod ([10]) reported the relative uncertainty matrix for the gains in the linearized model to be:

$$
k_{ij} : \begin{bmatrix} 31\% & 14\% & 35\% \\ 65\% & 11\% & 16\% \\ - & - & - \end{bmatrix} .
\tag{29}
$$

From the relative uncertainty matrix it is noted that a the LOAD/CFF transfer function has a relatively large uncertainty. With reference to this result another simulation run is performed in which the gain of the LOAD/CFF transfer function is perturbed. The gain of g_{21} is increased by 50% and the partial correlation plots are shown in Fig. 7.

From Fig. 7 it is clear that the significant mismatch is correctly identified to be in channel g_{21}. For this simulation run a reference change was once again made for the LOAD in order to ensure sufficient excitation. The OE model structure with order 3 was once again used to determine $\boldsymbol{G}_{u_i}$ and $\boldsymbol{G}_{e_j}$.

In practice a set-point change for LOAD is not very realistic. This is because the LOAD needs to be maintained at a specific value in order to achieve maximum throughput in the mill. Here the set-point change was made to ensure sufficient excitation in order to employ the model-plant mismatch algorithm.

A power peak-seeking throughput optimizer is sometimes employed ([16]) which should ensure sufficient excitation in the LOAD signal. If load set-point
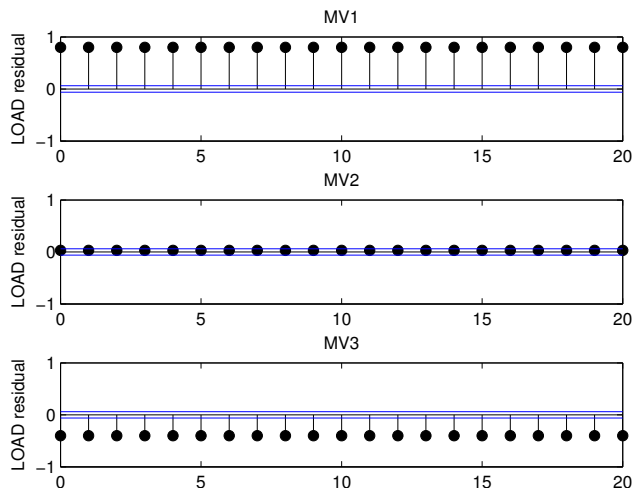
Figure 7: Partial correlation plots between the MVs and the LOAD residual for gain mismatch in g_{21}

changes are not common, sufficient excitation might result from parameter variations. Otherwise the control engineer may have to introduce set-point changes in the mill load when model-plant mismatch is suspected in order to generate data for the algorithm.

The presence of large non-stationary disturbances, which may be found in actual milling circuits, will also affect the accuracy of the MPM detection algorithm. The way [6] deal with disturbances is by firstly finding the disturbance free components of each signal before applying the MPM detection algorithm. This method is proven sufficient in the presence of large disturbances by [6], and once the disturbance free components of the signals are known, these may simply be used in the model update algorithm as discussed next.

Another common occurrence on industrial milling circuits is measurement

19

biases. As far as these may be seen as external disturbances they may also be handled as [6] does with other external disturbances. This is because they will not be correlated with the set-point changes made to ensure sufficient excitation.

6. Model update

The next question that arises is regarding the course of action to take once the model elements containing significant mismatch have been detected. One logical option is to re-identify the elements containing significant mismatch via an open-loop step test of the plant. It is however common for at least one of the model elements to be open-loop unstable which prompts additional consideration in the experiment design. This drawback can, among others, be eliminated through the use of a closed-loop identification procedure. The advantages of using closed-loop identification, as listed by [17], includes a reduction in the disruption of process operation and eliminating the need for manual control action.

The use of manual step tests to re-identify the model does require some effort on the part of the control engineer, but due to safety concerns such a supervised method is often advisable.

Irrespective of the way in which the new model is found, the objective is to minimize the magnitude of the residuals produced over the duration of the experiment. Given that the residual is the difference between the plant and model output, the modelling objective can be written as

$$\min_{\hat{G}} \sum_k \left| y(k) - \hat{G}u(k) \right| \tag{30}$$

$$s.t. \ \hat{G} \in \mathbb{G} \tag{31}$$

$$\theta_c(\hat{G}) \leq 0 \tag{32}$$

$$k_1 \triangleq 0 \tag{33}$$

$$k_f \triangleq T \tag{34}$$

where $y(k)$ and $\hat{G}u(k)$ (with $k \in [0, \ldots, T]$) are the plant and model outputs respectively. $\theta_c(\hat{G})$ is the set of inequality constraints on $\hat{G}$ (as described later) and $\mathbb{G}$ is the set of allowed model transfer functions. A discussion on the constraints for the allowed models will be given later in this section. The sum given in (30) will then tend to zero as $\hat{G} \to G$. This statement is however not free from consideration of disturbances. If unmeasured disturbances affect the plant output during the model re-identification an incorrect model could result.

Open and closed-loop model identification is well documented in [18, 19]. These methods can be implemented with the knowledge of the model elements containing significant mismatch, prompting only the need for partial re-identification. Another, possibly more intuitive, way of solving equation (30) is to directly employ a constrained minimization algorithm such as sequential quadratic programming [20]. Constrained minimization algorithms may not be as mathematically robust as open or closed-loop system identification techniques, but may be more easily employed with sufficient reliability if the number of model elements containing mismatch is small.

As open and closed-loop identification is broadly discussed elsewhere ([18, 19]), an explicit constrained minimization algorithm approach is pursued here. Such a solution will explicitly identify the new model based on

minimizing (30) where the parameters produced by the algorithm depend on the transfer functions containing mismatch and the structures of these transfer functions. Take for example the first illustration of MPM detection in the previous section where the time constants of g_{21} and g_{23} were increased. Here both transfer functions are in the form $g_{ij} = \frac{k_{ij}}{s+\alpha_{ij}}$ so the minimization algorithm should produce the values of k_{21}, k_{23}, α_{21} and α_{23} such that (30) is minimized. In the second instance shown, where the gain of g_{21} was increased, the minimization algorithm need only supply the values of k_{21} and α_{21} that causes (30) to be at a minimum.

Certain constraints on the parameters supplied by the minimization algorithm are imposed to ensure that reasonable results are obtained. When the parameters for a transfer function containing a time delay have to be calculated, it is logical to constrain the minimization algorithm to produce a time delay value that is non-negative. This is because the time delay can only be equal to or greater than zero. The constraint for the gain can be given as $k^* \cdot k > 0$, where k^* is the newly identified gain. This constraint will ensure that the new gain has the same sign as the original gain. This is done because it is not expected, at least not for this plant, that an input should suddenly start affecting an output in a different direction. The same constraint can be defined for time constants as stable poles are not expected to become unstable.

The overall MPM detection and model re-identification process is shown in Fig. 8. The detection of significant mismatch is firstly done based on the partial correlation analysis. Should the model contain significant MPM the model is re-identified through the model update algorithm. The control
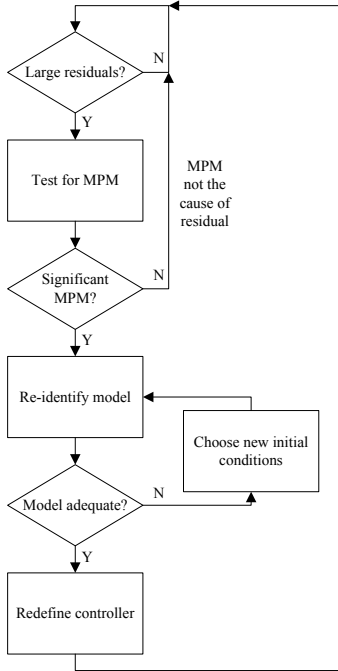
22

Figure 8: MPM detection and model re-identification procedure

engineer should then inspect the re-identified model to verify it's adequacy before the controller may be redefined with the new model.

The application of the minimization algorithm for partial re-identification will now be illustrated for the case where the gain of g_{21} was increased by 50%. The original transfer function and the new transfer function are respectively given by (35) and (36) to be

$$g_{21} = \frac{7.15 \times 10^{-4}}{s + 10^{-6}} \tag{35}$$

$$g_{21}^* = \frac{1.073 \times 10^{-3}}{s + 10^{-6}}. \tag{36}$$

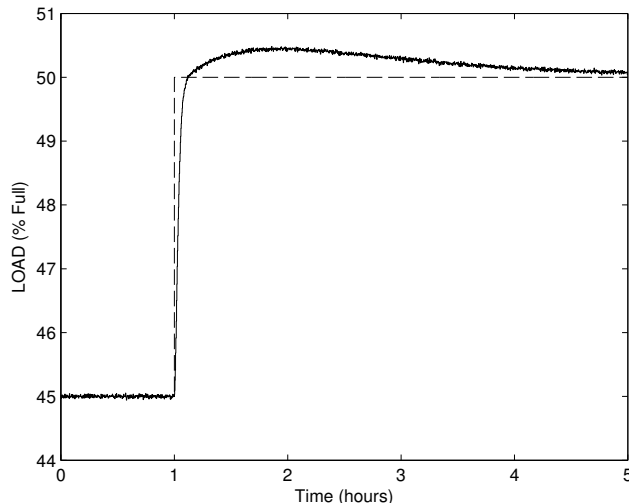With the model changed and the controller still defined according to the

Figure 9: Controller performance with model-plant mismatch present.

original model, the response to a step in the LOAD is as shown in Fig. 9. Clearly the mismatch causes deteriorated controller performance as the 2% settling time has increased to about four and a half hours. Usually a gain mismatch causes the model predictive controller to have this sluggish type of response. The form of the initial response depends on whether the gain was over- or underestimated, and thereafter it usually takes relatively long to achieve the desired set-point.

Next the sequential quadratic programming algorithm is used to determine the parameters (k_{21} and α_{21}) which minimize the difference between the plant and model outputs (as given by (30)). The parameters obtained from the minimization algorithm are

$$\hat{k}^* = 0.00107; \ \hat{\alpha}^* = 1 \times 10^{-6}. \tag{37}$$

These values are very close to the actual plant as was shown in (36). Should
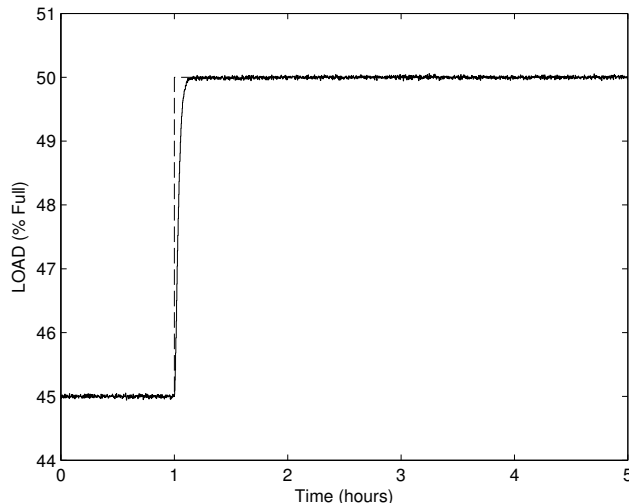
Figure 10: Controller performance with the re-identified model.

the controller now be redefined with the newly identified parameter values, the step response to a LOAD change is now as shown in Fig. 10. This step response is very similar to the original nominal performance which was shown in Fig. 2.

Although this example shows how the automatic model update algorithm handles a transfer function element that contains large uncertainty, it does not show the full potential of the algorithm. This is because the algorithm is basically only required to find the correct gain to minimize (30). A more stringent test on the algorithm is performed by changing

$$g_{11} = \frac{-2.4 \times 10^{-4}}{s + 0.5882} e^{-0.0111s} \tag{38}$$

to

$$g_{11}^* = \frac{-2.88 \times 10^{-4}}{s + 0.4706} e^{-0.0122s} \tag{39}$$

which is a 20% increase in the gain, a 20% decrease in the pole location value

25

and a 10% increase in the time delay. The sequential quadratic programming algorithm is now used to determine the parameters k_{11}, α_{11} and θ_{11} which minimize (30). The result supplied by the algorithm is

$$\hat{k}^* = -2.879 \times 10^{-4}; \ \hat{\alpha}^* = 0.4704; \ \hat{\theta}^* = 0.0121 \tag{40}$$

which is again very close to the true plant parameters.

Sufficiently exciting signals are once again required for the correct operation of the re-identification strategy.

7. Conclusion

This paper describes a simulation study of the application of model-plant mismatch detection and model re-identification to a ROM ore milling circuit under MPC control. The milling circuit model used is a linear time-invariant approximation of a fundamental milling circuit model. Model-plant mismatch, motivated from industrial experiments, is introduced in the model and its location in the multivariable matrix model is correctly detected. Next the new model is re-identified by making use of a sequential quadratic programming algorithm to explicitly minimize the residuals. For the MPM detection and re-identification strategies to work adequately, sufficiently exited signals are required – if this does not occur during normal plant operation, setpoint changes in the relevant outputs may have to be introduced. This study shows how the re-identification strategy can be automated, but it is not recommended that this procedure be applied blindly. Due to safety concerns the process engineer should firstly inspect the re-identified model before the controller is redefined therewith.

References

[1] D. Wei and I.K. Craig. Grinding mill circuits – A survey of control and economic concerns. *Int. J. Miner. Process.*, 90, pp. 56 – 66, 2009.

[2] S.J. Qin and T.A. Bagwell. A survey of industrial model predictive control technology. *Control Eng. Practice*, 11, pp. 733 – 764, 2003.

[3] D. Hodouin. Methods for automatic control, observation, and optimization in mineral processing plants. *J. Process Control*, 21, pp. 211 – 225, 2011.

[4] J. Yang, S. Li, X. Chen and Q. Li. Disturbance rejection of ball mill grinding circuit circuits using DOB and MPC. *Powder Technology*, 198, pp. 219 – 228, 2010.

[5] L.E. Olivier and I.K. Craig and Y.Q. Chen. Fractional order and BICO disturbance observers for a run-of-mine ore milling circuit. *J. Process Control*, 22, pp. 3 – 10, 2012.

[6] A.S. Badwe, R.D. Gudi, R.S. Patwardhan, S.L. Shah and S.C. Patwardhan. Detection of Model-Plant Mismatch in MPC applications. *J. Process Control*, 19, pp. 1305 – 1313, 2009.

[7] L.E. Olivier and Ian K. Craig. Parameter mismatch detection in a run-of-mine ore milling circuit under model predictive control. In: *Proc. 18th IFAC World Congress*, Milan, Italy, pp. 9929 – 9934, 2011.

[8] J.S. Conner and D.E. Seborg. Assessing the need for process re-

identification. *Industrial and Engineering Chemistry Research*, 44, pp. 2767 – 2775, 2005.

[9] L.C. Coetzee, I.K. Craig and E.C. Kerrigan. Robust Nonlinear Model Predictive Control of a Run-of-Mine Ore milling Circuit. *IEEE Trans. Control Syst. Technol.*, 18, pp. 222 – 229, 2010.

[10] I.K. Craig and I.M. MacLeod. Specification Framework for Robust Control of a Run-of-Mine ore Milling Circuit. *Control Eng. Practice*, 3, pp. 621 – 630, 1995.

[11] F.N. Shi and T.J. Napier-Munn. Effects of slurry rheology on industrial grinding performance. *Int. J. Mineral Processing*, 65, pp. 125 – 140, 2002.

[12] L. Ljung. *System Identification – Theory for the User*. Englewood Cliffs, NJ: Prentice Hall, 1987.

[13] L.C. Coetzee. Robust nonlinear model predictive control of a closed run-of-mine ore milling circuit. Ph.D. thesis, University of Pretoria, 2009.

[14] A. Bemporad, M. Morari and N.L. Ricker. Model predictive control toolbox for Matlab – Users guide, The Mathworks Inc., http://www.mathworks.com/access/helpdesk/help/toolbox/mpc/, 2004.

[15] D.E. Seborg, T.F. Edgar and D.A. Mellichamp. *Process Dynamics and Control*. Second Edition. Hoboken, NJ: Wiley, 2003.

[16] I.K. Craig, D.G. Hulbert, G. Metzner and S.P. Moult. Optimized multivariable control of an industrial run-of-mine circuit. *J. South African Institute of Mining and Metallurgy*, 92, pp. 169 – 176, 1992.

[17] Y. Zhu and F. Butoyi. Case studies on closed-loop identification for MPC. *Control Eng. Practice*, 10, pp. 403 – 417, 2002.

[18] P. Van den Hof. Closed-loop issues in system identification. *Annual reviews in control*, 22, pp. 173 – 186, 1998.

[19] Y.A.W. Shardt and B. Huang. Closed-loop identification with routine operating data: Effect of time delay and sampling time. *J. Process Control*, 21, pp. 997 – 1010, 2011.

[20] R. Fletcher. *Practical methods for optimization*. John Wiley and Sons, 1987.

Appendix A. Input models fit for time constant mismatch detection

The models used to find the component of each MV that is uncorrelated with all other MVs in the time constant mismatch detection step are listed here. They are all in the form

$$y(t) = \left[\frac{B(q)}{F(q)} \right] u(t - nk) + e(t) \tag{A.1}$$

with

$$B(q) = b_1 + b_2 q^{-1} + b_3 q^{-2} \tag{A.2}$$

and

$$F(q) = 1 + f_1 q^{-1} + f_2 q^{-2} + f_3 q^{-3}. \tag{A.3}$$

Finding the uncorrelated component of each MV requires fitting two models to the other MVs. The coefficients obtained when fitting the models are listed in Table A.1.

Table A.1: Coefficients for models fit while detecting time constant mismatch in g_{21} and g_{23}

Model	Coefficients		
G_{ui}	b_1	b_2	b_3
	f_1	f_2	f_3
$G_{u_{1,2}}$	0.005194	-0.009707	0.004515
	-2.922	2.845	-0.9228
$G_{u_{1,3}}$	5.152	-9.321	4.268
	-0.7825	0.1088	-0.204
$G_{u_{2,1}}$	40.36	-76.64	36.30
	-1.539	0.3329	0.2431
$G_{u_{2,3}}$	107	-213.3	106.3
	-0.9127	0.3225	-0.409
$G_{u_{3,1}}$	-0.5847	1.402	-0.7865
	-1.692	0.5728	0.144
$G_{u_{3,2}}$	-0.01034	0.02483	-0.01447
	-2.652	2.308	-0.656